Two-photon-absorption cross section of Nd^{3+} in yttrium aluminum garnet and yttrium lithium fluoride near 1.06 μm

L. L. Chase and Stephen A. Payne
Lawrence Livermore National Laboratory, University of California, P.O. Box 5508, Livermore, California 94550
(Received 25 July 1986)

We have measured the spectrally integrated two-photon-absorption (TPA) cross sections for the $^4I_{9/2} \rightarrow {}^4G_{7/2}$ transitions of Nd^{3+} and obtained values of 1.2×10^{-40} and 0.15×10^{-40} cm^4 for Nd^{3+}-doped yttrium aluminum garnet (YAG) and yttrium lithium fluoride (YLF), respectively. These results are in satisfactory agreement with theoretical calculations based on the properties of Nd^{3+} free-ion wave functions. The difference between YAG and YLF, however, is not accounted for by the free-ion theory and suggests that the intermediate-state energies and wave functions are considerably host dependent. In addition, we conclude, based on our measurements, that rare-earth TPA will not contribute significantly to either losses or the nonlinear refractive index in typical laser media employing rare-earth ions.

I. INTRODUCTION

Trivalent rare-earth ions exhibit $4f^n$-$4f^n$ transitions in the ir, visible, and/or uv spectral ranges. Judd[1] and Ofelt[2] have shown that the intensities of the $4f^n$-$4f^n$ transitions of an ion can be accurately fit with only three adjustable parameters.[3] This striking theoretical success was based on two unique attributes of trivalent rare-earth (R^{3+}) impurities: (a) the fact that the $4f$ wave functions retain much of their free-ion character, and (b) the feasibility of using the mathematical closure operation when describing the crystal-field-induced admixture of the atomic *nd* and *ng* wave functions into the $4f$ initial and final states. Judd-Ofelt theory involves the effects of two perturbations: one arising from the light wave, V_p; and the other from the odd components of the crystal field, V_{odd}. Although the form of V_p is well known, the nature of V_{odd} is quite difficult to determine. It depends sensitively on the positions of the ligands as well as on their electronic interaction with the R^{3+} ion. The result is that, although only three parameters are required to fit the spectral data, it is usually not possible to predict the absolute value of these parameters in an independent manner. Two-photon-absorption (TPA) spectroscopy provides an alternative method of investigating the nature of the spectral intensities of R^{3+} ions. Here, only the photon perturbation operator V_p is required, and V_{odd} need not be considered.

Axe has shown that allowed $4f^n$-$4f^n$ TPA transitions derive their intensity from the same even parity states as do the forbidden one-photon transitions.[4] In fact, he used the basic results of Judd-Ofelt theory to describe the TPA transition rate. We can therefore expect that it should be possible to calculate the absolute value of the TPA cross section solely from theoretical considerations. Axe's theory essentially predicts that only one parameter should be needed to fit the intensity of all $4f^n$-$4f^n$ TPA transitions between J levels (assuming that all crystal-field levels of the ground state are equally occupied).

In the present work we have experimentally measured the integrated TPA cross section of the $^4I_{9/2} \rightarrow {}^4G_{7/2}$ transitions of Nd^{3+}. We then used the theory of Axe to calculate this same cross section. These transitions are of particular significance because they occur for excitation near the typical 1.06 μm operating wavelength of a Nd^{3+} solid-state laser. There is, therefore, some possible practical significance to these two-photon transitions. They are a potential loss mechanism in Nd^{3+} lasers, and they may produce wavelength-dependent contributions to the nonlinear susceptibility and nonlinear refractive index. To our knowledge, the present work represents the first accurate measurement and theoretical modeling of an absolute TPA cross section for a $4f^n$-$4f^n$ transition of an R^{3+}-doped insulator.

Recently a number of workers have obtained extensive TPA spectra of the $^8S_{7/2} \rightarrow {}^6P, {}^6I, {}^6D$ transitions of the Gd^{3+} and Eu^{2+} ions, which have a $4f^7$ configuration.[5-10] Attempts to fit the relative intensities of the $4f^n$-$4f^n$ transitions to Axe's second-order theory were unsuccessful for the $^8S_{7/2} \rightarrow {}^6P, {}^6I$ transitions, and thus third- and fourth-order theories were developed to fit the data. Judd and Pooler have pointed out, however, that these transitions are largely TPA forbidden.

It has been shown that, within the Judd-Ofelt theory, the TPA cross sections are proportional to the square of a reduced matrix element, $\langle L,S;J||U^{(2)}||L',S',J'\rangle^2$.[4] In this work we employ the intermediate coupling matrix elements of $U^{(2)}$; the L and S designations indicate the major percentage of each term in Russell-Saunders coupling. For the $^8S_{7/2} \rightarrow {}^6P_J$ transitions, $\langle {}^8S_{7/2}||U^{(2)}||{}^6P_J\rangle^2 = 0.001\,166, 0.000\,470, 0.000\,016$ for $J = \frac{7}{2}, \frac{5}{2}, \frac{3}{2}$, respectively, while values near 1.0 are known to occur among the R^{3+} ions. Similarly the $^8S_{7/2} \rightarrow {}^6I$ transitions are predicted to have zero intensity, but instead are experimentally found to be of comparable magnitude to the $^8S_{7/2} \rightarrow {}^6P_{5/2}$ transition. Interestingly, the $^8S_{7/2} \rightarrow {}^6D$ transitions are found to be fairly well described by Axe's theory. These transitions, on the other hand, are characterized by somewhat larger reduced matrix elements; e.g.,

 ©1986 The American Physical Society

$\langle {}^4I_{9/2}||U^{(2)}||{}^6D_{9/2}\rangle^2=0.006$.

It is possible that the Judd-Ofelt theory breaks down at small values of

$\langle L,S;J||U^{(2)}||L',S',J'\rangle^2 \lesssim 0.005$.

Downer and Bivas[7] have made a "rough" measurement of the TPA cross section of a stark component of the ${}^8S_{7/2}\rightarrow{}^6P_{5/2}$ transition and have obtained a value of $\delta=2\times10^{-55}$ cm^{4}sec. This certainly is a particularly small cross section,[12] in agreement with the above discussion. For our case of the ${}^4I_{9/2}\rightarrow{}^4G_{7/2}$ transition of Nd^{3+},

$\langle {}^4I_{9/2}||U^{(2)}||{}^4G_{7/2}\rangle^2=0.055$,

and might be expected to be within the range of validity of the Judd-Ofelt-Axe TPA theory.

A number of TPA cross-section measurements have appeared in the literature. Skripko and Gintoft found values on the order of 10^{-56} and 10^{-57} cm^{4}sec for Eu^{3+}:CaF_2 and Sm^{3+}:CaF_2, respectively.[13] Again, we find that these transitions are largely forbidden. Apanasevich *et al.*[14] measured a value of $\sigma=6\times10^{-53}$ cm^{4}sec for the ${}^5I_8\rightarrow{}^3H_6$ transition of Ho^{3+}:CaF_2. This seems reasonable in light of the larger $\langle {}^5I_8||U^{(2)}||{}^3H_6\rangle^2$ value of 0.215 and the large bandwidth of 150 cm^{-1} in the CaF_2 host. They also found that $\delta=10^{-55}$ cm^{4}sec for the ${}^4I_{15/2}\rightarrow{}^4G_{11/2}$ transition of Er^{3+}:CaF_2. This result seems quite low since it involves a strongly allowed transition,

$\langle {}^4I_{15/2}||U^{(2)}||{}^4G_{11/2}\rangle^2=0.92$.

It is difficult to evaluate the significance of these cross sections because of the complex crystal-field splittings and broad spectra resulting from the charge-compensated, and possibly clustered, rare-earth sites in the fluorite crystals. Penzkofer and Kaiser[15] have measured the TPA cross section of the ${}^4I_{9/2}\rightarrow{}^4G_{7/2}$ transition of Nd^{3+}:glass and obtained a value of $\delta=2\times10^{-51}$ cm^{4}sec, which is extraordinarily large. In their calculation of the TPA cross section these authors apparently omitted the $\langle L,S;J||U^{(2)}||L',S';J'\rangle^2$ matrix element which would mean that their theoretical estimate is too large.

In view of the uncertainties regarding the magnitudes of the cross sections and the applicability of the Judd-Ofelt formalism to estimate them, as well as the possible practical importance of rare-earth TPA transitions, there is a need for an absolute measurement of allowed $4f^n$-$4f^n$ TPA cross sections for well-characterized ion-host combinations and an appropriate treatment of the theoretical equations. In Sec. II we describe our experimental methods in detail. We obtained the ${}^4I_{9/2}\rightarrow{}^4G_{7/2}$ sharp line TPA spectra of Nd^{3+} in yttrium aluminum garnet (YAG) and yttrium lithium fluoride (YLF), as well as the broader TPA of two glasses. We then describe a fairly accurate method of measuring the TPA cross section. We describe the techniques used to obtain the necessary experimental parameters, and then present the resulting cross sections and their error limits. We derive a general formula for calculating the TPA cross section of a R^{3+} ion in Sec. III. In Sec. IV we compare our experimental and theoretical results. In Sec. V we evaluate the potential nonlinear effects resulting from Nd^{3+} in a laser crystal. Our conclusions are summarized in Sec. VI.

II. EXPERIMENTAL TECHNIQUES AND RESULTS

A. Experimental setup

A diagram of the apparatus is shown in Fig. 1. We required tunable ir laser light in the region of 1.06 μm in order to obtain the TPA measurements of interest. To accomplish this we used the second harmonic of a Molectron MY-34 YAG laser to pump a Rhodamine-6G dye laser. The dye laser beam was focused into a 1-m cell filled with 600 psi of H_2 in order to generate the second-order Stokes-shifted beam, which was then recollimated. Appropriate cutoff filters were used to remove the dye laser and first-order Stokes-shifted laser light. The dye laser output had an energy of 6 mJ per pulse and the Raman-shifted (RS) beam contained 200 μJ per pulse, and was unpolarized. The RS output was arranged to be focused somewhat beyond the sample. By varying the distance between the 54-cm focal-length lens and the sample, the beam area at the sample could be varied. The ${}^4F_{3/2}\rightarrow{}^4I_{9/2}$ emission from the sample near 8750 Å was collected, passed through a monochromator, and then detected with a cooled GaAs photomultiplier tube. A portion of the incident beam served as a reference. Boxcar averaging was used to determine the detector signals, which were sent to a microcomputer and corrected for variations in the laser output by dividing the TPA signal by the square of the reference at each wavelength during a scan. Further details concerning the use of this setup are presented below.

B. Nd^{3+} spectra

In this section we present the ${}^4I_{9/2}\rightarrow{}^4G_{7/2}$ spectra of Nd^{3+}-doped hosts at 10 K, including those of YAG, YLF, and several glasses. At this temperature, only the lowest crystal-field component of the ${}^4I_{9/2}$ term is occupied. We require the form of these spectra in order to calculate the spectrally integrated cross section, $\int \delta d\nu$, for this transition. The two-photon spectrum of Nd^{3+}:YAG in Fig. 2 is composed of four sharp lines, the energies of

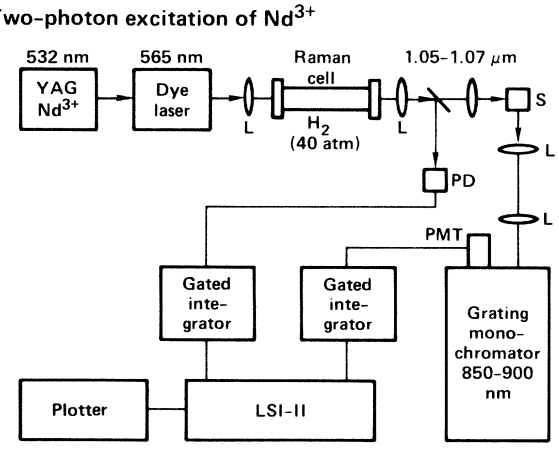

FIG. 1. Experimental setup used for two-photon excitation spectroscopy. *S* denotes sample, *L* denotes lens, PD denotes photodiode, PMT denotes photomultiplier tube.

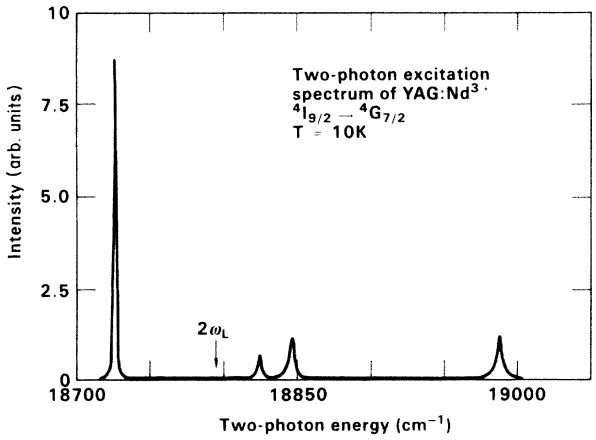

FIG. 2. Two-photon excitation spectrum of the $^4I_{9/2} \rightarrow {}^4G_{7/2}$ transitions of Nd^{3+}:YAG at 10 K. The Nd^{3+} $^4F_{3/2} \rightarrow {}^4I_{9/2}$ emission was monitored while the excitation source was scanned in the vicinity of one-half the operating wavelength $\omega_L = 1.064$ μm of a Nd^{3+}:YAG laser crystal.

which agree within a few wave numbers with those tabulated by Kaminskii.[16] This spectrum was recorded with $\mathbf{k}||[111]$ axis, using unpolarized light. Also noted in the figure is the energy of twice the operating frequency of a YAG:Nd^{3+} laser. Clearly, there is no overlap with the low-temperature TPA transitions, but at room temperature the thermal population of the ground-state multiplet and the thermal broadening does result in some degree of overlap.

Figure 3 contains the TPA spectra of Nd^{3+}:YLF, obtained with unpolarized light propagating along the c axis. The two major lines observed seem to be in disagreement with the results reported by da Gama *et al.*[17] We therefore checked our line positions with those obtained from our low-temperature absorption spectrum, and found good agreement. Note that the π and σ frequencies of laser operation are indicated on the figure. No other lines were observed from 18 900 cm^{-1} to 19 280 cm^{-1}.

Finally, we show in Fig. 4 the TPA spectra of Nd^{3+}-doped phosphate and silicate glasses. These TPA spectra are similar to the observed broad one-photon spectra. We can see that the operating frequency of a glass laser is typically resonant with an inhomogeneously broadened TPA transition. If the TPA cross section were as large as suggested by Penzkofer and Kaiser,[15] the TPA absorption would constitute a substantial loss mechanism.

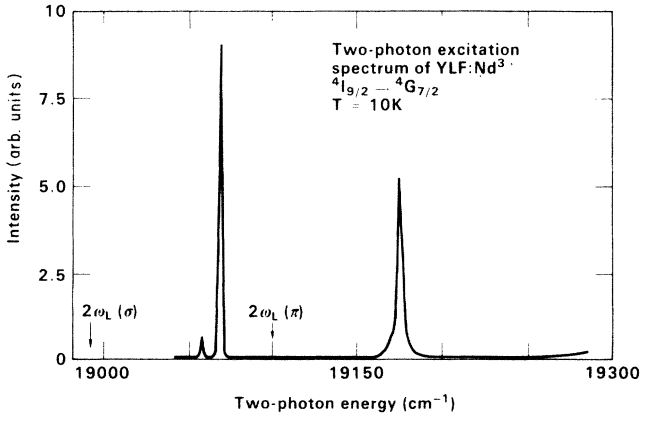

FIG. 3. Two-photon excitation spectra of Nd^{3+}:YLF. The Nd^{3+} $^4F_{3/2} \rightarrow {}^4I_{9/2}$ emission was monitored while the excitation source was scanned near one-half the operating wavelengths of a Nd^{3+}YLF laser (indicated as $2\omega_L$ in the figure).

C. Cross-section measurements

We have measured the TPA cross section by comparing the TPA-induced $^4F_{3/2} \rightarrow {}^4I_{9/2}$ luminescence signal that we observed using the Raman-shifted ir light with the luminescence observed using excitation from a weak one-photon transition at the visible dye laser frequency. Both YAG and YLF had such a residual one-photon absorption at the dye laser frequency, which gave a uniform excitation over the sample length.

We now develop the equations needed to apply this method. We assume that the laser pulse is Gaussian in space and time with a photon flux, $F(r,t)$ given by

$$F(r,t) = F_0 \exp(-r^2/r_0^2)\exp(-t^2/\tau^2) . \quad (1)$$

The observed luminescence signal due to TPA excitation is equal to

$$S_2 = \frac{K}{2} \int_{-\infty}^{+\infty} \int_0^l \int_0^{\infty} \left[-\frac{dF}{dz} \right] \times 2\pi r \, dr \, dz \, dt , \quad (2)$$

where we have integrated over r, the sample length l, and t. The factor of 2 accounts for the two photons needed to excite each ion, and K calibrates the overall detection efficiency of the $^4F_{3/2} \rightarrow {}^4I_{9/2}$ luminescence. The definition of the TPA cross section δ (cm^4 sec) is

$$\frac{dF}{dz} = -\delta F^2 N , \quad (3)$$

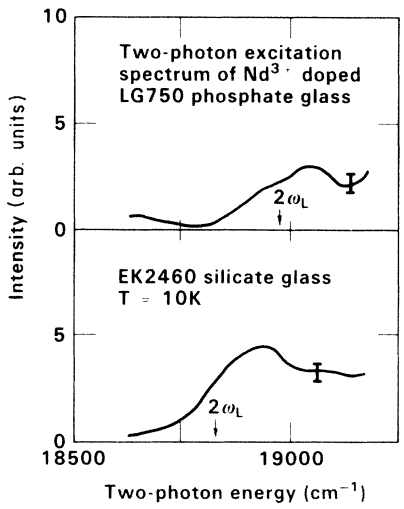

FIG. 4. Two-photon excitation spectra of Nd^{3+}-doped laser glasses. The broad, inhomogeneous excitation band is observed to be two-photon resonant with the energy of maximal stimulated gain at ω_L, for both the phosphate and the silicate glasses. The designations LG750 and EK2460 identify glass compositions made by Schott Glass Technologies and Eastman-Kodak, respectively.

where N is the number density of ions (cm^{-3}). The energy of a pulse can be written as

$$E = h\nu \int_{-\infty}^{+\infty} \int_0^{\infty} F_0 \exp(-r^2/r_0^2) \exp(-t^2/\tau^2) 2\pi r \, dr \, dt \ . \tag{4}$$

Performing the necessary integrations and substitutions, we obtain

$$S_2 = (2\pi)^{-3/2} \frac{K \delta N E_2^2 l}{2(h\nu_2)^2 r_0^2 \tau} \ , \tag{5}$$

where the subscript 2 refers to the two-photon excitation. Similarly the signal obtained with one-photon excitation can be written as

$$S_1 = \frac{K \alpha_1 E_1 l}{h\nu_1} \ , \tag{6}$$

where the one-photon absorption coefficient is defined as

$$\frac{dF}{dz} = -\alpha_1 F \ . \tag{7}$$

Combining Eqs. (5) and (6) to eliminate K and l, we get

$$\delta = \frac{2(2\pi)^{3/2} \alpha_1 r_0^2 \tau}{N} \left[\frac{S_2}{S_1} \right] \left[\frac{E_1/(h\nu_1)}{E_2^2/(h\nu_2)^2} \right] . \tag{8}$$

It is apparent that a number of independent measurements must be performed to determine δ. The techniques and results for each measurement are now described.

We determined the concentration N of Nd^{3+} in the YAG sample spectrophotometrically, using the absorption cross sections reported in Ref. 18. The Nd concentration in the YLF sample was determined by chemical analysis. The Nd concentration for YLF was used together with room-temperature optical-absorption data to deduce a cross section $\sigma = 3.1 \times 10^{-20}$ cm^2 for the line at 733 nm. The concentrations of Nd^{3+} are listed in Table I.

The pulse width of the laser τ was determined with a fast photodiode and a computer-controlled transient recorder. A 300-ps pulse from a N_2 laser was used to determine an instrument-limited time resolution of $\tau = 0.8$ ns. The RS beam had a measured width of $\tau = 1.7$ ns. The error limit of $\pm 50\%$ reflects the instability of the laser output.

As seen in Eq. (8) it is necessary to determine the radius r_0 of the beam at the sample. This measurement was performed two different ways. The first method involved using a computer-controlled vidicon to map out the profile of the beam at the focusing lens. Since the lens had a focal length of 54 cm and the beam waist occurred beyond the sample, geometric considerations could be used to determine the radius in the sample. Only the central 2 mm of the beam length in the sample was imaged onto the photomultiplier tube to avoid the variation of the beam radius along the sample. TPA measurements

TABLE I. Experimental values used to calculate the TPA cross section with Eq. (8); see text for identification of variables.

Quantity	Value	Method	Estimated error (%)
N, YAG	7.8×10^{19} cm^{-3}	Cross section from Ref. 18	±10
N, YLF	6.6×10^{19} cm^{-3}	Chemical analysis	±10
τ	1.7 ns	Photodiode	±50
α_1, YAG	0.097 cm^{-1}	Spectrophotometer	±20
	0.095 cm^{-1}	Laser excitation (see text)	±20
α_1, YLF	0.031 cm^{-1}	Spectrophotometer	±40
	0.035 cm^{-1}	Laser excitation	±20
r_0^2, 48 cm from lens, 54 cm focal length	2.8×10^{-3} cm^2	Vidicon	±30
	2.6×10^{-3} cm^2	Knife-edge scan	±30
$(S_2/E_2^2)/(S_1/E_1)$	Measured variable	Comparison of one-photon absorption and TPA signals	±50
Transmission of neutral density filters	2.35×10^{-5}	Spectrophotometer	±20

(described below) were obtained at four relative distances between the lens and the sample: 41.5, 44.8, 48.0, and 51.3 cm. The corresponding r_0 values were calculated to be 0.111, 0.082, 0.053, and 0.025 cm, respectively. We checked the radius at 48.0 cm by scanning a knife edge across the beam at the sample position and found good agreement with the calculated value (see Table I).

We now discuss how the one- and two-photon signals from the sample were compared. The RS output was tuned to the broadest line of the $^4I_{9/2} \rightarrow {}^4G_{7/2}$ transition in order to minimize the sensitivity of the signal to a small spectral mismatch. The focusing lens was first positioned to produce the largest radius on the sample and was adjusted laterally to maximize the luminescence signal. The TPA-induced luminescence signal and the laser pulse energy reference value were read from the boxcars. The reference diode was calibrated with an energy meter in a separate experiment. Next the YAG laser amplifier was turned off so that the energy was below the threshold for stimulated Raman generation, and the color filters were replaced with several calibrated neutral density filters. The residual Nd^{3+} absorption at the same dye laser wavelength utilized to generate the Stokes beam was sufficient to provide for substantial one-photon excitation of the Nd^{3+} ions. We checked that this excitation produced the same luminescence spectrum and lifetime that is normally observed in YAG and YLF. (Note that the actual absorption coefficient α_1 at the dye laser wavelength was determined in a separate experiment.) The laser beam position was then readjusted to maximize this signal, since the Stokes and the dye laser beams did not travel exactly the same path. This sequence was repeated a second time. Then this procedure was utilized for the three other beam radii mentioned above. The entire run was repeated to check for a longer term variation. The standard deviation of the ratio of the two- and one-photon signals, after correction for the value of r_0^2, was $\pm 50\%$.

Finally, we require the value of the absorption coefficient α_1 at the dye laser wavelength. We obtained the values listed in Table I with a spectrophotometer. Since α_1 was chosen to be rather small in order to obtain uniform excitation, we also checked these measurements with an additional experiment using the laser system. This was done by comparing the luminescence produced when the dye laser was tuned to the frequency used to normalize the TPA measurements with the luminescence produced when the laser was tuned to a frequency at which α was larger, and more accurately measured spectrophotometrically. As seen in Table I, good agreement with the spectrophotometric results was obtained.

All of the measurements were performed at 10 K. We found that the TPA measurements were impossible at room temperature since the thermal population of the $^4I_{11/2}$ state leads to a one-photon luminescence signal that is much larger than the TPA signal.

The values of δ (cm^4 sec) calculated with Eq. (8) are listed in Table II. The starred numbers are the actual measurements. The other δ values were determined from the relative peak heights in Figs. 2 and 3. In order to compare the overall cross sections for YAG and YLF it is necessary to integrate over the final crystal-field-split states. Thus using Figs. 2 and 3 and the data in Table II, we obtain the spectrally integrated cross section for the $^4I_{9/2} \rightarrow {}^4G_{7/2}$ transition to be $\Delta = \int \delta \, d\nu = 1.2 \times 10^{-40}$ cm^4 for Nd^{3+}:YAG and 0.15×10^{-40} cm^4 for Nd^{3+}:YLF. In the next section we will calculate the value of Δ using Judd-Ofelt-Axe theory.

III. THEORY

The integrated TPA cross section Δ can be calculated from[19–21]

$$\int \delta \, d\nu = \sum_f (2\pi\alpha)^2 \, | S_{gf} \, |^2 \rho^{(2)} L^4 / n^2 \, , \tag{9}$$

where $\alpha = \frac{1}{137}$ is the fine-structure constant. The Lorentz field correction is

$$L = (n^2 + 2)/3 \, , \tag{10}$$

TABLE II. Energies, widths, and two-photon cross sections δ for each of the lines of the $^4I_{9/2} \rightarrow {}^4G_{7/2}$ transition for Nd^{3+}:YAG and Nd^{3+}:YLF. The values with asterisks are the actual measurements of δ, while the other values were determined with reference to Figs. 2 and 3. The integrated cross sections Δ were determined using the data in this table. (FWHM denotes full width at half maximum.)

Crystal	TPA energy (cm^{-1})	FWHM (10^{10} sec^{-1})	δ (10^{-52} cm^4 sec)	$\Delta = \int \delta \, d\nu$ and error limits (10^{-40} cm^4)
YAG	18 991	10.5	2.8*	1.2
	18 847	8.3	2.6	(0.4 to 4)
	18 827	8.3	1.3	
	18 727	3.5	18	
YLF	19 070	3.6	1.5	0.15
	19 174	10.5	0.9*	(0.05 to 0.5)

where n is the refractive index at the photon energy $h\nu$. $\rho^{(2)}$ is the correlation function and can be written as

$$\rho^{(2)}=\langle A^4\rangle/\langle A^2\rangle^2 , \tag{11}$$

where A is the vector potential of the laser field. $\rho^{(2)}=2$ or 1 for completely incoherent or coherent light, respectively. S_{gf} is defined by

$$S_{gf}=h\nu\sum_i \frac{\langle f\,|\,\hat{\mathbf{e}}_1\cdot\mathbf{r}\,|\,i\rangle\langle i\,|\,\hat{\mathbf{e}}_2\cdot\mathbf{r}\,|\,g\rangle}{E_{ig}-h\nu}+(1\leftrightarrow 2) , \tag{12}$$

where g, f, and i are, respectively, the ground, final, and intermediate states; $\mathbf{r}$ is the electron coordinate; and $\hat{\mathbf{e}}_i$ is the unit polarization vector of the laser light for photons $i=1,2$. Axe[4] has shown that, for trivalent rare-earth ions, the Judd-Ofelt theory[1,2] is applicable and that for a transition from $|J,M\rangle$ to $|J',M'\rangle$, S_{gf} can be written as

$$S^{(K)}_{JM,J',M'}=-(-1)^{J'-M'}\begin{pmatrix} J' & 2 & J \\ -M' & K & M\end{pmatrix}\langle L'S'J'||U^{(2)}||LSJ\rangle$$
$$\times\sum_{n'',l''}\left[\frac{(l+l''+1)(3l-l''+1)(4l-2l''+1)}{6(l+l'')(l+l''+2)}\right]^{1/2}\frac{h\nu}{\Delta E(n''l'')}\,|\langle nl\,|\,r\,|\,n''l''\rangle|^2 , \tag{13}$$

where n,l correspond to the $4f$ initial and final states, K denotes a spherical tensor polarization component, the $U^{(2)}$ reduced matrix elements can be found in various tabulations,[3,22] $\Delta E(n''l'')$ is the energy separation of the $n''l''$ intermediate configuration from the virtual level at $E=h\nu$, and the last factor is a radial integral.

We are interested only in transitions from the lowest crystal-field level of the $^4I_{9/2}$ term to all of the crystal-field levels of the $^4G_{7/2}$ term. It is easily shown that the value of the integrated cross section Δ obtained by summing over the $^4G_{7/2}$ levels is independent of the detailed wave functions of the $^4G_{7/2}$ levels, since the crystal-field splitting is very small compared with both the photon energy and the denominator in Eq. (12). We therefore perform the sum over the unsplit states $|J',M'\rangle$ of $^4G_{7/2}$ and use the known wave functions, $\psi=\sum_M a_M|J,M\rangle$, for the lowest Kramers doublet of YAG:Nd^{3+},[23]

$$\psi_\pm=0.258\,|\,\tfrac{9}{2},\pm\tfrac{3}{2}\rangle+0.9686\,|\,\tfrac{9}{2},\mp\tfrac{5}{2}\rangle ,$$

and YLF:Nd^{3+},[24]

$$\psi_\pm=0.448\,|\,\tfrac{9}{2},\pm\tfrac{9}{2}\rangle+0.668\,|\,\tfrac{9}{2},\mp\tfrac{7}{2}\rangle-0.562\,|\,\tfrac{9}{2},\pm\tfrac{1}{2}\rangle .$$

The integrated two-photon-absorption cross section is then obtained from (9) using

$$\sum_{g,f}|S_{gf}|^2=\sum_{M'=-7/2}^{+7/2}\left[\sum_{M,K}a_M S^{(K)}_{JM,J'M'}e^{(2)}_K\right]^2 , \tag{14}$$

where $e^{(2)}_K$ are the spherical tensor polarization components that are easily obtained from the rectangular polarization components of the incident laser light. For the special case of unpolarized light propagating along $\langle 111\rangle$ in YAG, all Nd^{3+} sites are equivalent and, as in the case of YLF, no additional sum over sites is required. The $e^{(2)}_K$ were calculated for each of the two equal, uncorrelated polarization components of the laser and the two resulting contributions to Eq. (14) were summed after squaring. We used

$$\langle {}^4I_{9/2}||U^{(2)}||{}^4G_{7/2}\rangle^2=0.055$$

(Ref. 22) and assumed that $\rho^{(2)}=2$, since the RS beam has a frequency-pulse-width product of (0.5 cm^{-1})(1700 psec)=800 psec cm^{-1}, whereas the Fourier-transform-limited product is 5 psec cm^{-1}.

It is not possible to perform the complete sum over intermediate states in Eq. (12). We have therefore used separate expressions to calculate the TPA cross sections, Δ_d and Δ_g, assuming that either the $4f^25d$ or $4f^2ng$ configurations, respectively, are the intermediate states. We obtain

$$\Delta_d=4.8\times10^{-4}\left[\frac{h\nu}{\Delta E(5d)}\right]^2|\langle 4f\,|\,r\,|\,5d\rangle|^4B\frac{L^4}{n^2} , \tag{15a}$$

$$\Delta_g=1.5\times10^{-4}\left[\frac{h\nu}{\Delta E(ng)}\right]^2|\langle 4f\,|\,r^2\,|\,4f\rangle|^2B\frac{L^4}{n^2} , \tag{15b}$$

where B is a factor dependent on the propagation directions in the samples, the laser polarizations, and the ground-state wave functions. In Eq. (15b) we have made use of a closure relation[1] to eliminate the $\langle 4f\,|\,r\,|\,n''g\rangle$ integrals, which are unknown.

IV. COMPARISON OF CALCULATED AND MEASURED CROSS SECTIONS

At the present time, only the free-ion values of the matrix elements and energy denominators in Eqs. (15) are available. Judd[1] interpolated Rajnak's[25] calculated values of the radial integrals for Pr^{3+} and Tm^{3+} to obtain values for Nd^{3+} and Er^{3+}. More recently, however, Rajnak[26] and co-workers have computed new values of $\langle 4f\,|\,r\,|\,5d\rangle=0.39$ Å and $\langle 4f\,|\,r^2\,|\,4f\rangle=0.31$ Å^2 for Nd^{3+}, and we employed these in our calculations. Using $\Delta E(5d)=58\,000$ cm^{-1} in Eq. (15a), we obtain the values of Δ_d shown in Table III for YAG, YLF, and a "typical" glass, for which we have averaged the cross section over all $2J+1$ sublevels of the $^4I_{9/2}$ ground term. The values

TABLE III. Calculated and experimental two-photon cross sections for the $^4I_{9/2} \rightarrow {}^4G_{7/2}$ transition of Nd^{3+}-doped hosts. The values of the parameters used in Eq. (15) are indicated.

Sample	Δ_d (10^{-40} cm^4) $\Delta E(5d)=58\,000$ cm^{-1} $\langle 4f \mid r \mid 5d \rangle = 0.39$ Å	Δ_g (10^{-40} cm^4) $\Delta E(ng)=167\,000$ cm^{-1} $\langle 4f \mid r^2 \mid 4f \rangle = 0.31$ Å^2	Experimental (10^{-40} cm^4)
YAG $B=0.012$ $L^4/n^2=2.97$	1.1	0.17	1.2
YLF $B=0.022$ $L^4/n^2=2.19$	1.4	0.22	0.15
Glass $B=0.02$ $L^4/n^2=1.8$	1.1	0.17	

of parameters used in Eqs. (15) for each host are also given in the table. For the *ng* configurations, we have used Judd's[1] suggested value of $\Delta E(ng) \sim 1.67 \times 10^5$ cm^{-1}, which is a rough estimate of the ionization energy of the Nd^{3+} ion in a coordinate complex. The resulting values of Δ_g in Table III are somewhat smaller than Δ_d. In view of the fact that the use of free-ion parameters to characterize the behavior of these outer *d* and *g* orbitals is likely to be only a crude approximation, a possibly greater relative influence of the *ng* configurations cannot be discounted. There is, in fact, some existing evidence for the importance of these *ng* configurations as intermediate states in optical transitions. Krupke[27] applied the Judd-Ofelt theory to the optical-absorption spectra for a set of rare earths in Y_2O_3 and LaF_3, and argued, based on his results, that the value of $\langle 4f \mid r \mid 5d \rangle^2$ is reduced by about an order of magnitude in a crystalline environment, whereas the $\langle 4f \mid r^2 \mid 4f \rangle$ integral is slightly increased. The sensitivity of the former matrix element to radial expansion of the $5d$ wave function results from the fact that the $5d$ function has both positive and negative parts, and the $4f$ function is positive everywhere. This can lead to rapid variations in the matrix element because of cancellations. More recently, Becker *et al.*[28] obtained evidence, based on the degree of asymmetry of electronic Raman transitions of rare-earth ions, that the $5d$ and *ng* contributions to two-photon processes in solids are about equal. They argued that the $5d$ and *ng* orbitals are likely to be largely composed of ligand orbitals, rather than free-ion wave functions, and there is therefore no reason to expect one kind of orbital to predominate.

Considering the experimental and theoretical uncertainties, we regard our measured absolute cross sections as being in satisfactory, order-of-magnitude agreement with the theoretical values. On the other hand, since the same properties of the $5d$ and *ng* orbitals are assumed for YAG and YLF, and the values of *B* and *L* correct for the other factors determining the cross sections, it is striking that the ratios of measured and calculated cross sections differ by about an order of magnitude for the two crystals. We believe that the ratios of the cross sections are accurate to better than a factor of 3. Our results therefore imply that there is a considerable host dependence to the TPA cross sections. Such a host dependence is consistent with the idea expressed above that the $5d$ and *ng* orbitals may be strongly mixed with ligand orbitals. Apparently, the net effect of this mixing is to cause larger TPA cross sections for the more covalent oxide coordination of YAG. This is in agreement with the observed lower energy for the $4f^{n-1}5d$ levels of rare earths in oxides compared with fluorides.[29] Similarly, the ionization energy would be lower in an oxide, and, as a result, the $4f^2ng$ energy denominators in Eqs. (15) are also expected to be smaller. Considering, however, the possible involvement of other factors, such as the changes in sign of the $5d$ wave function in the spatial region where the $4f$ functions are large, it is not clear that increasing covalency will always lead to increasing TPA cross sections. Recently, it has been pointed out by Reid and Richardson[30] that virtual optical transitions on the ligand ions (related to the ligand polarizability), combined with the coupling of the ligand electrons to the rare-earth ion, may alter TPA selection rules and cross sections. This higher-order mechanism for two-photon processes may be of importance[30] in the highly forbidden TPA transitions studied by Downer *et al.*,[5-9] but its significance for allowed transitions, such as those investigated in this work, is uncertain. This mechanism would, however, also produce larger TPA cross sections for coordination by the more polarizable oxygen anions.

V. TPA-INDUCED LOSS AND NONLINEAR DISPERSION

The significance of TPA processes as a loss mechanism in lasers employing rare-earth ions can be evaluated by employing Eq. (3) for a typical upper limit to the intensity of a laser system, $I = Fh\nu \sim 10^9$ W/cm^2 and a concentration $N \sim 10^{20}$ cm^{-3}. The effective absorption coefficient at the peak of the largest TPA line in YAG:Nd^{3+} is

$$\frac{1}{F}\frac{dF}{dz} = \frac{\delta I N}{h\nu} \sim 10^{-3} \text{ cm}^{-1} .$$

This shows that, even in media where a sharp, strong TPA transition precisely overlaps the laser transition, the resulting loss is negligible at moderate-to-high intensities. (For the unlikely case of a strongly allowed TPA line in a neat rare-earth compound, however, absorption coefficients exceeding 0.1 cm^{-1} are possible.) A previous report[15] of significant loss due to TPA of Nd^{3+} in laser glass, where the large linewidths would lead to much lower values of δ, is clearly in error.

It has been suggested recently[31,32] that TPA transitions of rare-earth and transition-metal ions may produce a dispersive contribution to the nonlinear refractive index, n_2(TPA), that is comparable to that of the host medium. This wavelength-dependent n_2(TPA) could either be added to or subtracted from the nonlinear index of the host, depending on the frequency of the incident wave relative to the TPA resonance frequency. To investigate the possible significance of these effects, we note the relationships of the TPA cross section δ and the nonlinear index n_2 to the nonlinear susceptibility $\chi^{(3)}_{\text{eff}}$, which is a linear combination of tensor components of $\tilde{\chi}^{(3)}$ determined by the polarization of the propagating wave:

$$\delta = \frac{96\pi^2\hbar\omega^2}{Nn^2c^2}\text{Im}\chi^{(3)}_{\text{eff}} , \tag{16}$$

$$n_2 = \frac{12\pi}{n}\text{Re}\chi^{(3)}_{\text{eff}} . \tag{17}$$

For a Lorentzian TPA resonance, $\chi^{(3)} \propto (2\omega - \omega_0 + i\gamma)^{-1}$, and the frequency-dependent n_2 is related to the peak cross section $\delta_{\max}$ by combining Eqs. (16) and (17) to obtain

$$n_2(\text{TPA}) = \frac{\delta_{\max} Nnc^2}{8\pi\hbar\omega^2}\frac{\varepsilon}{\varepsilon^2+1} , \tag{18}$$

where $\varepsilon = (2\omega - \omega_0)/\gamma$. Using the values $\delta_{\max} = 1.8\times10^{-51}$ cm^4 sec and $N \sim 10^{20}$ cm^{-3} typical of YAG:Nd^{3+}, we find a maximum contribution to n_2(TPA) of about 2×10^{-15} esu. This is a factor of 10^2 lower than the n_2 values for typical optical laser materials. Just as was the case for absorptive losses, rare-earth TPA will only make significant contributions to n_2 near resonance with strongly allowed TPA transitions in concentrated rare-earth crystals. The idea of canceling the nonlinearity of the host with the anomalous n_2 due to rare-earth TPA (Refs. 31 and 32) seems to us to be a very unlikely possibility.

VI. CONCLUSIONS

The measured cross sections for allowed $^4I_{9/2} \rightarrow {}^4G_{7/2}$ TPA transitions of Nd^{3+} in YAG and YLF are in satisfactory order-of-magnitude agreement with calculations employing free-ion parameters. The measured total cross sections were, however, an order of magnitude smaller in YLF than in YAG. This difference, which is larger than the estimated experimental error in the relative cross sections, implies a strong host dependence for the cross sections.

From the magnitudes of the cross sections, we conclude that even the sharp, allowed TPA lines of rare-earth ion impurities are unlikely to contribute significantly to losses or nonlinear dispersion in typical laser media.

ACKNOWLEDGMENTS

We wish to thank Dr. W. F. Krupke for sharing his insights with us, and Professor K. Rajnak for critically reading this manuscript. We are also grateful to Gary Wilke for his technical assistance in all aspects of this work. This work was performed under the auspices of the Division of Materials Sciences of the Office of Basic Energy, Sciences, U.S. Department of Energy, and the Lawrence Livermore National Laboratory under Contract No. W-7405-ENG-48.

[1]B. R. Judd, Phys. Rev. **127**, 750 (1962).
[2]G. S. Ofelt, J. Chem. Phys. **37**, 511 (1962).
[3]W. T. Carnall, P. R. Fields, and B. G. Wybourne, J. Chem. Phys. **42**, 3797 (1965); W. T. Carnall, P. R. Fields, and K. Rajnak, *ibid.* **49**, 4412 (1968).
[4]J. D. Axe, Jr., Phys. Rev. **136**, A42 (1964).
[5]M. Dagenais, M. Downer, R. Neumann, and N. Bloembergen, Phys. Rev. Lett. **46**, 561 (1981).
[6]M. C. Downer, A. Bivas, and N. Bloembergen, Opt. Commun. **41**, 335 (1982).
[7]M. C. Downer and A. Bivas, Phys. Rev. B **28**, 3677 (1983).
[8]M. C. Downer, C. D. Cordero-Montalvo, and H. Crosswhite, Phys. Rev. B **28**, 4931 (1983).
[9]B. Bloembergen, J. Lumin. **31/32**, 23 (1984).
[10]C. D. Cordero-Montalvo, Phys. Rev. B **31**, 5433 (1985).
[11]B. R. Judd and D. R. Pooler, J. Phys. C **15**, 591 (1982).
[12]See W. L. Smith, in *CRC Handbook of Laser Science and Technology,* edited by M. J. Weber (CRC, Boca Raton, 1986), Vol. 3, Pt.1, for a listing of known two-photon cross sections.
[13]G. A. Skripko and R. I. Gintoft, J. Appl. Spectrosc. **24**, 245 (1977).
[14]P. A. Apanasevich, R. I. Gintoft, V. S. Korolkov, A. G. Makhanek, and G. A. Skripko, Phys. Status Solidi B **58**, 745 (1973).
[15]A. Penzkofer and W. Kaiser, Appl. Phys. Lett. **21**, 427 (1972).
[16]A. A. Kaminskii, *Laser Crystals* (Springer-Verlag, New York, 1981).
[17]A. A. S. da Gama, G. F. de Sa, P. Porcher, and P. Caro, J. Chem. Phys. **75**, 2583 (1981).
[18]T. Kushida, H. M. Marcos, and J. E. Geusic, Phys. Rev. **167**, 289 (1968).
[19]B. Honig, J. Jortner, and A. Szoke, J. Chem. Phys. **46**, 2714 (1967).
[20]W. M. McClain and R. A. Harris, in *Excited States,* edited by E. C. Lim (Academic, New York, 1977), Vol. 3.
[21]B. Dick and G. Hohlneicher, J. Chem. Phys. **76**, 5755 (1982).

[22]R. Reisfeld and C. K. Jorgenson, *Lasers and Excited States of Rare Earths* (Springer-Verlag, New York, 1977).
[23]F. P. Safaryan, Fiz. Tverd. Tela (Leningrad) **20**, 1563 (1978) [Sov. Phys.—Solid State **20**, 903 (1978)].
[24]D. Sengupta and J. O. Artman, J. Chem. Phys. **53**, 838 (1970).
[25]K. Rajnak, J. Chem. Phys. **43**, 847 (1965).
[26]W. T. Carnall, J. V. Beitz, H. Crosswhite, K. Rajnak, and J. B. Mann in *Systematics and the Properties of Lanthanides*, edited by S. P. Sinha (Kluwer, Hingham, 1983).
[27]W. F. Krupke, Phys. Rev. **145**, 325 (1966).
[28]P. C. Becker, N. Edelstein, B. R. Judd, R. C. Leavitt, and G. M. S. Lister, J. Phys. C **18**, L1063 (1985).
[29]K. S. Bagdasarov, I. S. Volodina, A. I. Kolomiltsev, M. L. Meil'man, and A. G. Smagin, Kvant. Elektron. (Moscow) **9**, 1158 (1982) [Sov. J. Quantum Electron. **12**, 731 (1982)]; S. P. Chernov, L. I. Devyatkova, O. N. Ivanova, A. A. Kaminskii, V. V. Mikhailin, S. N. Rudnev, and T. V. Uvarova, Phys. Status Solidi A **88**, K169 (1985).
[30]M. F. Reid and F. S. Richardson, Phys. Rev. B **29**, 2830 (1984).
[31]G. B. Altshuler, V. B. Karasev, S. A. Kozlov, and A. V. Ovchinnikov, Pis'ma Zh. Tekn. Fiz. **9**, 799 (1983) [Sov. Tekn. Phys. Lett. **9**, 344 (1983)].
[32]G. B. Altshuler and S. A. Kozlov, Kvant. Elektron. (Moscow) **12**, 698 (1985) [Sov. J. Quantum Electron **15**, 459 (1985)].